nature communications

Article

https://doi.org/10.1038/s41467-025-56353-4

Rescue RM/CS-AKI by blocking strategy with one-dose anti-myoglobin RabMAb

Received: 24 June 2024

Accepted: 13 January 2025

Published online: 26 January 2025

Check for updates

Xinyue Wang[1,2,3,10], Ning Li[1,2,3,4,10] ✉, Lu Han[5,6,10], Ou Qiao[1,2,3,10], Xin Chen[1,2,3,7], Pengtao Wang[8], Lancao Zhang[1,2], Yingjie Hou[1,2,3,7], Fengjiao Bao[1,2,3], Herui Hao[1,2,3], Sania Saeed[1,2,3,7], Li Zhang[1,2,3], Zizheng Li[1,2,3], Xiaohong Duan[1,2,3], Shuquan Rao[5,6] ✉, Zichuan Liu[7,9] ✉ & Yanhua Gong[1,2,3,4] ✉

Rhabdomyolysis or Crush syndrome-related AKI (RM/CS-AKI) has high mortality, and there is no effective early on-site treatment method. The critical pathogenic factor of RM/CS-AKI is the excessive free myoglobin (Mb) in blood circulation. Here, based on the concept of creating a "mobile barrier", we develop an anti-Mb rabbit monoclonal antibody (RabMAb) with high specificity, affinity, stability, and broad species reactivity. A single dose of anti-Mb RabMAb injection is sufficient for emergency rescue in both homologous and heterologous RM/CS-AKI male animal models. The main goal of blocking the passage of free Mb through the glomerular filtration barrier has been achieved by using the anti-Mb RabMAb, which has a long-term stable therapeutic effect within 14 days and promotes phagocytosis of Mb. The optimal administration strategy, pharmacokinetic analysis, toxicity evaluation for anti-Mb RabMAb, and the distribution of its immune complexes in RM/CS-AKI mice are investigated. Thus, we develop effective prevention and control strategies for RM/CS-AKI.

Acute kidney injury (AKI) is a syndrome characterized by sudden loss of kidney function that causes 2 million deaths worldwide each year and has become a global health problem[1,2]. So far, its diagnosis, treatment, and prevention remain significant challenges for clinicians, incredibly intensive care physicians[3]. Rhabdomyolysis-related AKI accounts for approximately 5–10% of intensive care unit cases[4], which can be divided into traumatic rhabdomyolysis and non-traumatic rhabdomyolysis based on the cause of the disease[5]. Non-traumatic rhabdomyolysis is hereafter abbreviated as RM. RM is ubiquitous in daily life[6], including narcotic addiction[7], alcoholism[8], excessive exercise[9], and high fever[10]. Traumatic rhabdomyolysis, also known as Crush Syndrome, is hereafter abbreviated as CS. The earliest recorded case of CS occurred in 1277 when Pope John XXI was buried under the rubble due to a collapsed house. Despite being rescued alive, he ultimately died on the seventh day after being rescued[11]. Until World War II, Bywaters and Beall first proposed the "Crush Syndrome" concept[12]. CS always has a very high incidence and mortality rate during wartime, even in today's peaceful era[13,14]. Millions of people worldwide still suffer from disaster emergencies, such as earthquakes[15], collapses[16], traffic accidents[17], war, etc[18,19]. In particular, recently, on February 6, 2023, a series of earthquakes occurred in Türkiye, causing 50783 deaths and 115353 injuries[20]. It is reported that 37% of the victims who

[1]School of Disaster and Emergency Medicine, Faculty of Medicine, Tianjin University, No. 92 Weijin Road, Nankai District, Tianjin 300072, China. [2]Institute of Disaster and Emergency Medicine, Faculty of Medicine, Tianjin University, Tianjin, China. [3]Medical School, Faculty of Medicine, Tianjin University, Tianjin, China. [4]Key Laboratory for Disaster Medicine Technology, Tianjin, China. [5]State Key Laboratory of Experimental Hematology, National Clinical Research Center for Blood Diseases, Haihe Laboratory of Cell Ecosystem, Institute of Hematology & Blood Diseases Hospital, Chinese Academy of Medical Sciences & Peking Union Medical College, Tianjin 300020, China. [6]Tianjin Institutes of Health Science, Tianjin 301600, China. [7]School of Pharmaceutical Science and Technology, Faculty of Medicine, Tianjin University, Tianjin, China. [8]Department of Severe Illnese Medicine, Tianjin First Center Hospital, Tianjin 300192, China. [9]Frontiers Science Center for Synthetic Biology (Ministry of Education), Tianjin University, Tianjin, China. [10]These authors contributed equally: Xinyue Wang, Ning Li, Lu Han, Ou Qiao. ✉e-mail: lining620@tju.edu.cn; raoshuquan@ihcams.ac.cn; zichuan.liu@tju.edu.cn; gongyanhua@tju.edu.cn

https://doi.org/10.1038/s41467-025-56353-4

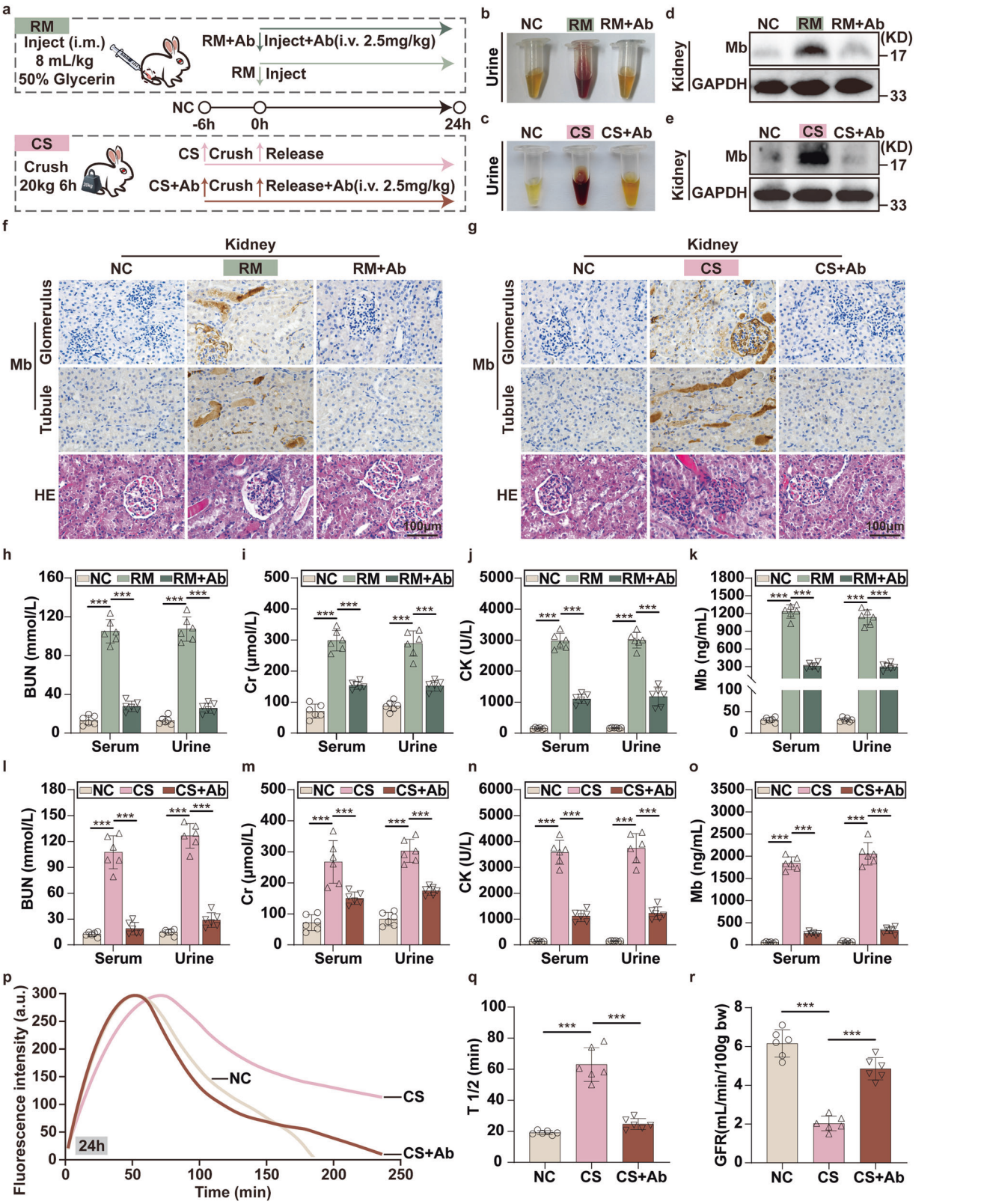

were treated in Türkiye's Kayseri State Hospital suffered from CS. Among them, 58% of CS patients still die after hospitalization, and 30% require continuous dialysis[21]. Therefore, CS and related complications are undoubtedly the most severe problems post-earthquake patients face. These remind us to seize the first "72 h gold time window" of emergency rescue and reduce the mortality rate of CS at the disaster site, which is the key to treatment.

RM/CS is mainly caused by direct or indirect damage to muscle cells, which leads to the release of cellular contents into the blood circulation[22], ultimately resulting in severe complications such as hyperkalemia[23] and Myoglobin-related AKI (Mb-AKI)[24]. Especially, AKI caused by Mb is the main complication of RM/CS and a critical factor in inpatient mortality[25,26]. The pathophysiology of RM/CS-AKI is excessively free Mb from blood circulation exceeds the body's

Fig. 1 | Medium-sized animal RM/CS-AKI model rabbits were rescued with anti-Mb RabMAb. a Experimental design diagram of anti-Mb RabMAb treatment for RM/CS-AKI model rabbits. **b**, **c** Urine was collected after 24 h of RM/CS-AKI model rabbits injected with anti-Mb RabMAb. **d**, **e** WB detection of Mb abundance in the kidneys of RM/CS-AKI model rabbits after anti-Mb RabMAb treatment. GAPDH was used as the loading control. $n = 3$ biological replicates for each group (**f**, **g**) Immunohistochemistry staining was used to detect the Mb casts distribution in the kidney tissue, and HE staining was used to analyze the kidney injury of RM/CS-AKI model rabbits treated with anti-Mb RabMAb. **h**–**o** BUN, Cr, CK, and Mb concentration in rabbit serum and urine (p-values for pairs all indicated from left to right: $p < 0.0001$). **p** Representative images of transcutaneous disappearance curves of FITC-sinistrin excretion. The x-axis represents time, and the y-axis represents the relative transcutaneous fluorescence. **q** Terminal half-life ($T_{1/2}$) of FITC-sinistrin excretion (p-values for pairs all indicated from left to right: $p < 0.0001$). **r** GFR values of each group of rabbits were calculated from the $T_{1/2}$ of FITC-sinistrin (p-values for pairs all indicated from left to right: $p < 0.0001$). Graph bars represent mean ± SD, and dots indicate individual data points for $n = 3$ biological replicates with 2 technical replicates per group in (**h**–**o**, **q**, **r**). Two-way ANOVA for (**h**–**o**) and one-way ANOVA for (**q**, **r**) followed by Tukey's multiple comparisons test were used to identify the differences. * $p < 0.05$, ** $p < 0.01$, *** $p < 0.001$. Source data are provided as a Source Data file.

clearance capacity and then accumulates in the kidney, inducing renal injury due to Mb toxicity, intratubular cast formation, and renal vasoconstriction[27,28].

Early treatment of RM/CS patients is crucial in reducing the incidence and mortality of AKI after a large-scale casualty event occurs[29,30]. At present, in-hospital treatments of Mb-AKI (RM/CS-AKI) mainly focus on the removal of toxic substances, including renal replacement therapy (RRT)[31]. However, RRT primarily relies on large equipment, which is severely lacking in large-scale emergencies, and its removal efficiency for Mb needs to be higher[32]. Based on this critical rescue situation, research has turned to early, portable, practical drugs for emergencies. Although there is currently an emergency drug for hyperkalemia, there is still no medication to reduce excessive free Mb in blood circulation. For excessive free Mb with significant nephrotoxicity in peripheral blood circulation, medical staff still do not have early effective on-site targeted detoxification drugs. Therefore, developing new medicines that can clear excess free Mb is crucial for alleviating the progression of RM/CS-AKI.

Antibody therapy is ideal for targeting pathogenic factors to achieve causal treatment. Several preclinical explorations at the level of small animals have used antibodies (anti-RAGE, anti-HMGB-1) to antagonize systemic inflammatory response factors after crush injury functionally[33–35]. However, the most essential initiating nephrotoxic injury factor (Mb) released after rhabdomyolysis wasn't directly neutralized or antagonized. Therefore, we proposed a concept of creating a "mobile barrier" to protect the glomerular filtration barrier: anti-Mb IgG antibody (~150 KD) binds to the free Mb (~17 KD) in the blood circulation to form immune complexes, which have large sizes will not be able to pass through the primary membrane aperture of the glomerular filtration barrier (~69 KD) physically blocking Mb renal toxicity.

Here, we developed a novel strong specificity, excellent affinity, superior stability, and broad species reactivity anti-Mb rabbit monoclonal antibody (RabMAb). Anti-Mb RabMAb one-dose injection alleviated RM/CS-AKI by blocking Mb from passing through the glomerular filtration barrier and promotes phagocytosis of Mb in both homologous (rabbit) and heterologous (mouse) animal models. We determined the optimal administration dosage, mode, and timing of anti-Mb RabMAb treatment and completed preliminary pharmacokinetic analysis and toxicity evaluation in RM/CS-AKI mice. As a single-dose administration antibody for emergency treatment, it has a stable therapeutic effect for at least 14 d or more. It is adequate during the first "72 h gold time window" of emergency rescue. In the future, the combined administration of anti-Mb RabMAb and potassium-lowering drugs is expected to more effectively relieve RM/CS-AKI and reduce the mortality rate of emergency events.

Results

Medium animal RM/CS-AKI model rabbits were rescued with anti-Mb RabMAb

We successfully developed a novel rabbit-derived IgG full-length monoclonal neutralizing antibody against Mb (anti-Mb RabMAb). The anti-Mb RabMAb has broad species reactivity with mice, rats, rabbits (Supplementary Fig. 1a), and humans[36]. Meanwhile, the anti-Mb RabMAb could specifically bind to native Mb from mouse, rat, and rabbit skeletal muscle lysates, RM/CS-AKI mouse serum and kidney lysates (Supplementary Fig. 1b–d). In addition, the binding kinetics of anti-Mb RabMAb to full-length recombinant immunogen Mb was determined by surface plasmon resonance (SPR). The equilibrium dissociation constant (K_D) value is 0.9409 pM, suggesting the Mb-specific high-binding affinity (Supplementary Fig. 1e). Moreover, the anti-Mb RabMAb exhibited good stability at −80, 4, 25, 37, and 55 °C for 24 h, or at 25 °C for 0, 0.5, 1, 2, 3, 7, 14, 21, and 28 d, or freeze-thaw cycles for 0, 1, 3, 5, and 7 times (Supplementary Fig. 1f, g). For more detailed information about the anti-Mb RabMAb, please refer to our early research[36]. These results demonstrated that the anti-Mb RabMAb had broad species reactivity, strong specificity, excellent affinity, and superior stability.

To determine whether the anti-Mb RabMAb could preserve the kidney structure and function of RM/CS-AKI, we injected the anti-Mb RabMAb into a homologous medium-sized RM/CS-AKI animal model (rabbits) (Fig. 1a). Severe red urine (myoglobinuria instead) occurred in the RM/CS-AKI model rabbits, while the anti-Mb RabMAb groups showed significant relief after 24 h of antibody injection (Fig. 1b, c). The WB results showed that a large amount of the nephrotoxic protein Mb accumulated in the kidneys of RM/CS-AKI model rabbits, while the content of Mb in the kidney of the anti-Mb RabMAb group was substantially reduced (Fig. 1d, e). Meanwhile, IHC results showed obvious Mb casts form in glomerulus and tubules of RM/CS-AKI groups, while these phenomena were significantly alleviated in the anti-Mb RabMAb group (Fig. 1f, g and Supplementary Fig. 2a, b, d, e). Moreover, anti-Mb RabMAb treatment improves the abnormal renal tissue structure in the RM/CS-AKI groups, including glomerular atrophy, renal tubular intracavitary cells exfoliated, brush border structure disappearance (Fig. 1f, g and Supplementary Fig. 2c, f). In addition, compared with the RM/CS-AKI groups, the contents of BUN, Cr, CK, and Mb in the serum and urine of the anti-Mb RabMAb groups were noticeably decreased, indicating kidney injuries and function were considerably ameliorated (Fig. 1h–o). Furthermore, the glomerular filtration rate (GFR) of the anti-Mb RabMAb group was markedly increased, and renal function was improved (Fig. 1p–r). Overall, anti-Mb RabMAb can alleviate renal injury in homologous medium-sized animal RM/CS-AKI model rabbits.

Anti-Mb RabMAb alleviates kidney injury of RM/CS-AKI mice by decreasing Mb accumulation

We further performed anti-Mb RabMAb treatment in heterologous RM/CS-AKI model mice (Fig. 2a). Excitingly, the mouse survival rate of the RM group or CS group was approximately 25% or 5% at 72 h after modeling, while the anti-Mb RabMAb group had a high survival rate of about 90% or 75%, respectively (Fig. 2b, c). Compared with the RM/CS-AKI group, the expression level of the renal injury marker NGAL and the content of Mb in the kidneys decreased in the anti-Mb RabMAb group (Fig. 2d, e). Moreover, Mb staining in the proximal renal tubules that contour was showed by LTL labeled brush border of the anti-Mb RabMAb group was substantially reduced compared to the RM/CS-AKI group and RM/CS-AKI + PBS group (Fig. 2f, g). Similarly, the levels of Mb and renal injury marker NGAL and KIM-1 were strongly reduced in the anti-Mb RabMAb group compared to the RM/CS-AKI group or RM/

https://doi.org/10.1038/s41467-025-56353-4

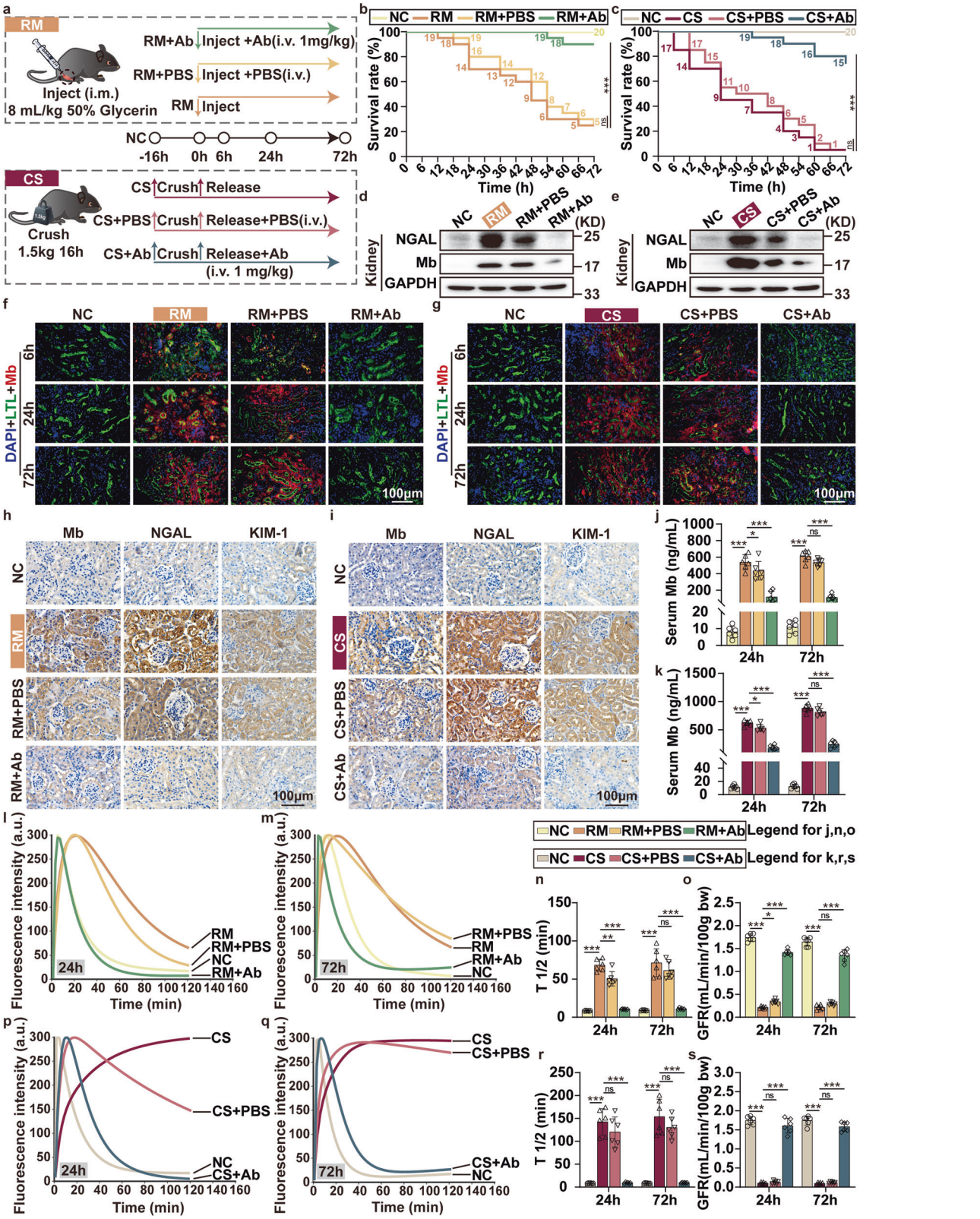

CS-AKI + PBS group (Fig. 2h, i and Supplementary Fig. 3a–f). Meanwhile, the change of Mb in blood circulation among the groups was consistent with the kidney (Fig. 2j, k). Moreover, anti-Mb RabMAb treatment decreased the BUN and CK levels in the serum (Supplementary Fig. 3g–j). In addition, compared to the RM/CS-AKI group, the GFR of the anti-Mb RabMAb group was highly increased at 24 h and 72 h, indicating a marked improvement in renal function (Fig. 2l–s). Meanwhile, the urinary protein analysis revealed an increase in both the large protein fraction albumin (glomerular injury marker, 66 KD) and the fraction of small-molecular-size proteins (tubular injury marker including 33 KD α1-microglobulin or 11.8 KD β2-microglobulin) in the RM-AKI group (Supplementary Fig. 3k). This indicated that there was an increase in glomerular permeability and tubular damage (or mixed pattern) in RM-AKI model mice. However, anti-Mb RabMAb

Fig. 2 | Anti-Mb RabMAb alleviates kidney injury of RM/CS-AKI mice by decreasing Mb accumulation. a Experimental design diagram of anti-Mb RabMAb treatment for RM/CS-AKI model mouse. **b**, **c** Survival rate curves of each group of mice within 72 h. The cumulative incidence estimate was used to calculate the probability of survival rate as a function of time. The log-rank test was used to compare survival curves. $n = 20$ for biological replicates. **d**, **e** WB detection of NGAL expression and Mb accumulation in the kidneys in each group. GAPDH was used as the loading control. $n = 3$ biological replicates for each group. **f**, **g** Immunofluorescence staining detected the Mb distribution and contents in the kidney tissue. The nuclei were stained with DAPI (blue). The lotus tetragonolobus lectin (LTL, green) labeled brush border showed the proximal tubule contour. **h**, **i** Immunohistochemistry staining detected the distribution of Mb, NGAL, and KIM-1 in the kidney tissue. $n = 3$ for biological replicates. **j**, **k** Mb concentration in mouse serum. **l**, **m**, **p**, **q** Representative images of transcutaneous disappearance curves of FITC-sinistrin excretion at 24 h and 72 h. The x-axis represents time, and the *y*-axis represents the relative transcutaneous fluorescence. **n**, **r** Terminal half-life ($T_{1/2}$) of FITC-sinistrin excretion. **o**, **s** GFR values of each group of mice were calculated from the excretion $T_{1/2}$ of FITC-sinistrin. Graph bars represent mean ± SD, and dots indicate individual data points for $n = 6$ for biological replicates per group in (**j**, **k**, **n**, **o**, **r**, **s**). Two-way ANOVA for (**j**, **k**, **n**, **o**, **r**, **s**) followed by Tukey's multiple comparisons test were used to identify the differences. * $p < 0.05$, ** $p < 0.01$, *** $p < 0.001$, ns: no significance. The exact *p*-value can be found in the Source Data file. Source data are provided as a Source Data file.

treatment reduced the leakage of large and small-molecular-size proteins, returning to levels nearly consistent with those of the NC group (Supplementary Fig. 3k). Overall, anti-Mb RabMAb can reduce Mb content in renal tubules by neutralizing free Mb in the blood, thereby alleviating renal injury, improving kidney function and increasing the survival rate of RM/CS-AKI model mice.

Anti-Mb RabMAb prevents free Mb from entering renal tubular epithelial cells and promotes macrophage phagocytosis of Mb

To investigate the mechanism of anti-Mb RabMAb in alleviating kidney injury, we expressed and purified mouse Mb. The IP results demonstrated that purified Mb could be specifically bound by anti-Mb RabMAb (Fig. 3a). According to the pathogenesis of RM/CS-AKI, immortalized tubular epithelial cells (TECs) from mice (TCMK-1 cells) were treated with Mb to mimic cell model of RM/CS-AKI[25,37]. The IC_{50} value of mouse ferrous Mb in TCMK-1 cells was 231.9 μM (Fig. 3b). Combined with previous experience[25], 200 μM ferrous Mb lower than the IC_{50} value was finally used for subsequent cell experiments. Immunofluorescence staining showed that Mb accumulation in TCMK-1 cells increased in a time-dependent manner after 200 μM ferrous Mb treatment, peaking at 6 h (Fig. 3c). Subsequently, with the extension of time, the cells were seriously damaged. Therefore, we selected TCMK-1 cells incubated with 200 μM ferrous Mb for 6 h to mimic the cell model of RM/CS-AKI. Meanwhile, CCK8 results showed that 0.001–3.2 mg/mL anti-Mb RabMAb had almost no cytotoxicity on TCMK-1 cells, and cell viability was always higher than 95% (Fig. 3d). Next, 200 μM ferrous Mb was mixed with anti-Mb RabMAb at different concentration range from 0.001 to 3.2 mg/L to treat TCMK-1 cells. The corresponding EC_{50} value was calculated to be ~ 0.02 mg/mL, and the minimum effective concentration of anti-Mb RabMAb that resulted in more than 95% cell viability was 0.2 mg/mL (Fig. 3e). Thus, we finally selected the anti-Mb RabMAb concentration of 0.2 mg/mL for subsequent in vitro experiments.

TCMK-1 cells were co-treated with 200 μM ferrous Mb and 0.2 mg/mL anti-Mb RabMAb or rabbit IgG for 6 h. Immunofluorescence results showed that Mb accumulation in TCMK-1 cells was significantly reduced in the Mb + Ab group compared with the Mb and Mb + IgG groups (Fig. 3f). These results indicated that anti-Mb RabMAb could rapidly neutralize extracellular Mb, thereby preventing its entry into TCMK-1 cells and blocking its toxicity. But where did the immune complex formed after anti-Mb RabMAb capturing free Mb in the body go? Have mononuclear macrophages scavenged it in vivo? To answer this question, RAW 264.7 cells were treated with 200 μM ferrous Mb and 0.2 mg/mL anti-Mb RabMAb or DYN (inhibition of macrophage phagocytosis). Immunofluorescence staining showed that the Mb group began to swallow Mb at 1 h, and Mb is not completely metabolized by macrophages until 48 h (Fig. 3g, h and Supplementary Fig. 4). In contrast, the phagocytosis of Mb by RAW 264.7 cells in Mb + Ab group was extremely accelerated, and the phagocytic effect was evident at 0.5 h. It is noteworthy that the intracellular Mb content peaked at 2–4 h, and was almost completely degraded and metabolized at 12 h (Fig. 3h and Supplementary Fig. 4). These suggested that when anti-Mb RabMAb captured Mb, the immune complex was quickly carried to the macrophage, which is specifically engulfed and degraded, significantly improving its metabolic efficiency. For the Mb + Ab + DYN group, the immune complexes existed until 48 h because macrophage phagocytosis function was prevented (Fig. 3h and Supplementary Fig. 4). In conclusion, anti-Mb RabMAb can effectively neutralize and prevent free Mb from entering renal tubular epithelial cells, while promoting macrophage to phagocytose and degrade Mb.

The optimal administration strategy for anti-Mb RabMAb therapy RM-AKI mice

After confirming the effectiveness and mechanism of anti-Mb RabMAb therapy RM/CS-AKI, we further investigated the optimal administration strategy for anti-Mb RabMAb, including dosage, mode, and timing. We first explored the effects of a range of anti-Mb RabMAb concentrations (0.05, 0.1, 0.25, 0.5, 1, 5, 10, and 20 mg/kg) on renal function under intravenous administration mode (Fig. 4a). Compared to the RM group, anti-Mb RabMAb groups significantly improved in kidney function (Fig. 4b–d and Supplementary Fig. 5a, b), had lower Mb and CK contents in the blood (Fig. 4e and Supplementary Fig. 5c), lower Mb accumulation and NGAL and KIM-1 expression in kidney (Fig. 4f and Supplementary Fig. 5d, e), mild pathological change (Supplementary Fig. 5f). Among them, the kidney function evaluation gold standard GFR assays showed that kidney function improved even though in a 0.1 mg/kg dose of anti-Mb RabMAb, and the 1 mg/kg dose had the best therapeutic effect (Fig. 4b–f and Supplementary Fig. 5a–f). Next, to analyze routes of administration, we injected 1 mg/kg anti-Mb RabMAb by an i.v., i.p., i.m., or s.c. (Fig. 4g). Four administration modes all decreased the levels of BUN, Cr, CK, and Mb in the blood (Supplementary Fig. 5g–i and Fig. 4h), as well as the accumulation of Mb and the expression of NGAL and KIM-1 in the kidneys (Fig. 4i and Supplementary Fig. 5j, k). Meanwhile, the renal tissue structure was not abnormal (Supplementary Fig. 5l), and the renal function was noticeably improved (Fig. 4j–l). Among them, the therapeutic effect of i.v. and i.p. was superior to that of i.m. and s.c. The i.v. the method was slightly better, but the difference was insignificant with i.p (Fig. 4h–l and Supplementary Fig. 5g–l). Thus, we chose i.v. as the optimal route of administration. Finally, we explored the optimal timing of administration (Fig. 4m). The results of blood biochemistry, qPCR, WB, HE, and GFR showed that compared with RM mice, i.v. injection of 1 mg/kg anti-Mb RabMAb within 24 h before and after modeling remarkably improved renal function and alleviated kidney injury (Fig. 4n–r and Supplementary Fig. 5m–r). The best therapeutic effect was observed when the anti-Mb RabMAb was given immediately after modeling. Therefore, the optimal administration strategy of the anti-Mb RabMAb was the immediate intravenous injection of 1 mg/kg upon RM/CS-AKI, which can maximize the improvement of kidney function and reduce kidney injury.

Tissue distribution, pharmacokinetic analysis, and toxicity evaluation of anti-Mb RabMAb in RM/CS-AKI mice

The in vivo tissue distribution characteristics and metabolism were observed over 14 days by a single intravenous injection of

https://doi.org/10.1038/s41467-025-56353-4

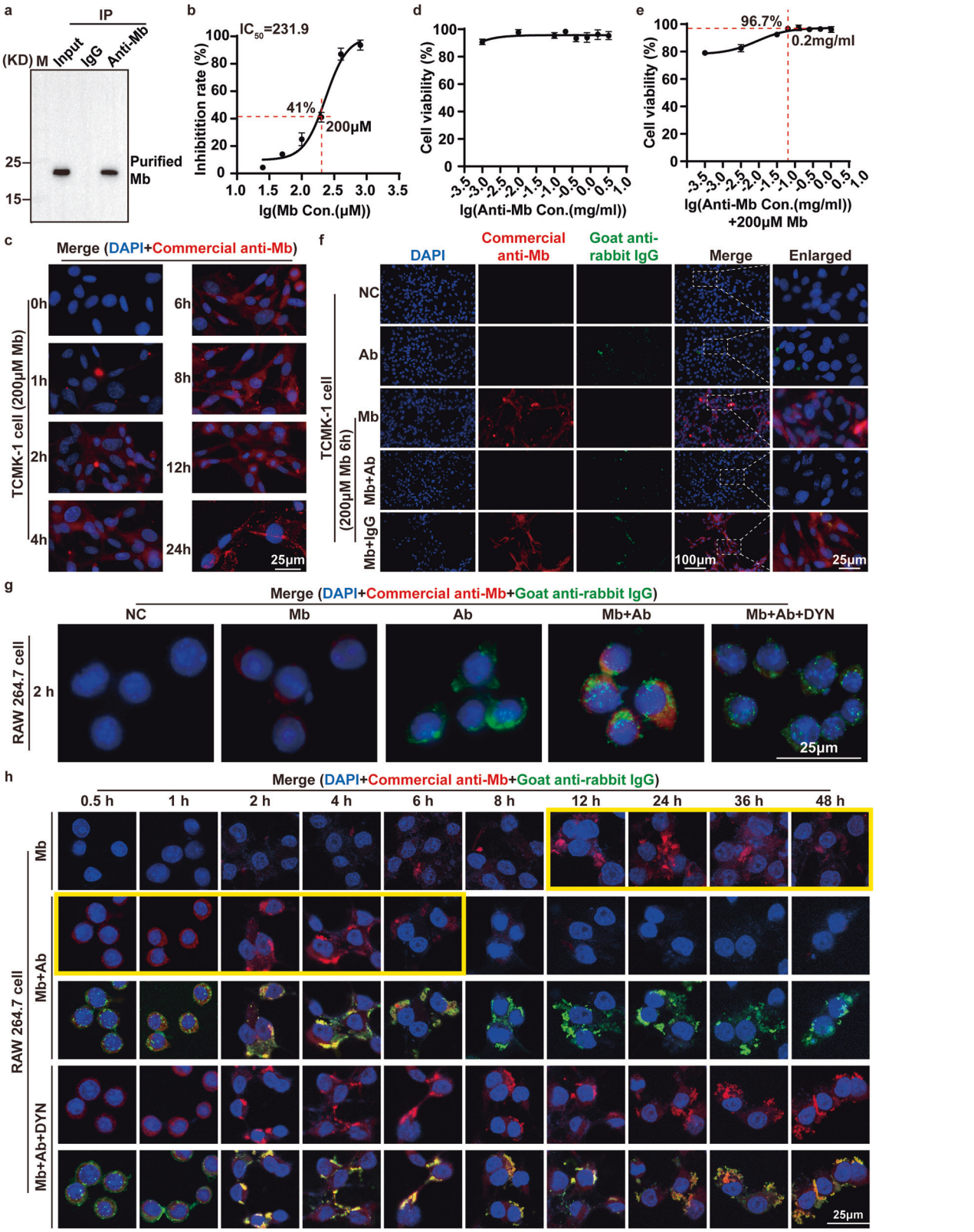

Cy5-labeled anti-Mb RabMAb. In vivo imaging showed that anti-Mb RabMAb is primarily distributed in organs with abundant blood flow and relatively leaky vasculature (heart, liver, spleen, lung, kidney) and damaged muscles exhibiting Mb leakage (Fig. 5a). The distribution in the brain and normal muscle was very shallow (Fig. 5a). The fluorescence signal reached its peak approximately 12–24 h in RM/CS-AKI group after administering Cy5-labeled anti-Mb RabMAb (Fig. 5a). Meanwhile, kidneys and damaged muscles of RM/CS-AKI mice have higher fluorescence signal intensity while signals were weak within hearts, and almost no fluorescence signals were detected in normal muscle tissues of NC mice (Fig. 5b–e). In other words, the anti-Mb RabMAb did not reside in mice's hearts or normal muscle tissues, while selectively targeted damaged muscles exhibiting Mb leakage and kidneys with significant Mb

Fig. 3 | Anti-Mb RabMAb prevents free Mb from entering renal tubular epithelial cells and promotes macrophage phagocytosis of Mb. **a** Immunoprecipitation of the anti-Mb RabMAb with the His-Mb, which was expressed and purified by our research group. IgG antibody acted as a negative control. **b** Using CCK8 assay to detect the inhibition rate of TCMK-1 cells treated with different concentration gradients ferrous His-Mb (25, 50, 100, 200, 400, and 800 μM) for 6 h, and calculate the IC_{50} value. **c** Representative confocal microscopy images of TCMK-1 cells treated with 200 μM ferrous His-Mb at different times (0, 1, 2, 4, 6, 8, 12, and 24 h). **d** CCK8 assay detected the survival rate of TCMK-1 cells treated with different concentrations of anti-Mb RabMAb (0.001, 0.01, 0.1, 0.2, 0.4, 0.8, 1.6, and 3.2 mg/mL). **e** CCK8 assay detected the survival rate of TCMK-1 cells treated with 200 μM ferrous His-Mb and different concentrations of anti-Mb RabMAb (0.001, 0.01, 0.1, 0.2, 0.4, 0.8, 1.6, and 3.2 mg/mL). Data are presented as mean ± SD, and $n = 3$ biological replicates for each group in (**b**, **d**, **e**). **f** Representative confocal microscopy images of TCMK-1 cells were treated with 200 μM ferrous His-Mb and 0.2 mg/mL anti-Mb RabMAb/IgG for 6 h. **g** Representative confocal microscopy images of RAW 264.7 cells which were treated with 200 μM ferrous His-Mb, 0.2 mg/mL anti-Mb RabMAb, and macrophage membrane dynamic protein inhibitor DYN for 2 h. **h** Representative confocal microscopy images of RAW 264.7 cells treated with 200 μM ferrous His-Mb, 0.2 mg/mL anti-Mb RabMAb, and macrophage membrane dynamic protein inhibitor DYN for different times (0.5, 1, 2, 4, 6, 8, 12, 24, 36, and 48 h) to observe the phagocytosis of macrophages. The nuclei were stained with DAPI (blue), the His-Mb were stained with commercial anti-Mb (red), and the anti-Mb RabMAb/IgG antibody were stained with goat anti-rabbit IgG (green) in (**f**–**h**). Representative images of $n = 3$ biological replicates for each group. Source data are provided as a Source Data file.

accumulation, and then neutralized and promoted the degradation of Mb.

Quantitative analysis of fluorescence signals from various organs at different time points is consistent with the previous description. Anti-Mb RabMAb reached the peak within 1 d and remained in the kidney of RM/CS-AKI mice for a longer time than that of NC mice (Fig. 5c). Meanwhile, it was noticeably increased in the damaged muscle of RM/CS-AKI mice, reaching a peak at about 5 d and being completely metabolized at 14 d (Fig. 5d). Moreover, anti-Mb RabMAb consistently maintained a low distribution level in the hearts of all groups (Fig. 5e). In addition, the metabolism of anti-Mb RabMAb in the liver, spleen, and lung of RM/CS-AKI mice was slightly slowed down (Supplementary Fig. 6a–c). Meanwhile, the pharmacokinetic analysis of anti-Mb RabMAb supported the in vivo tissue fluorescence distribution of the anti-Mb RabMAb (Fig. 5f, g). From the plasma concentration-time profiles, the maximum plasma concentration (C_{max}) and the time to reach C_{max} (T_{max}) were obtained (Fig. 5f, g). The NC, RM-AKI, and CS-AKI groups need similar time to reach C_{max} (2.50 ± 1.97 h, 2.50 ± 1.97 h, 2.67 ± 2.58 h, respectively). The mean terminal elimination half-life ($T_{1/2}$) of the anti-Mb RabMAb was 8.88 ± 0.29 d, 11.11 ± 0.60 d, 11.74 ± 0.54 d in NC, RM-AKI, and CS-AKI group, respectively (Fig. 5g). In addition, area under the serum concentration-time curve from time 0 to infinity [$AUC_{(inf)}$], volume of distribution (Vz), and plasma clearance (Cl) were obtained in Fig. 5g.

As anti-Mb RabMAb was distributed to varying degrees in mice's kidneys, muscles, hearts, liver, spleen, and lungs after intravenous injection, we further explore whether anti-Mb RabMab could cause side effects on these vital organs. Compared to the NC group, the RM-AKI+Ab group and CS-AKI + Ab group showed no apparent pathological damage in the kidney, muscle, heart, liver, spleen, and lung within short-term 72 h (6 h, 24 h, and 72 h) or 14 d, respectively (Supplementary Fig. 7a–n). Moreover, qPCR results showed that endothelial activation markers *P-selectin* and *Vcam-1* mRNA expression in the CS/RM-AKI + Ab group was reduced in both target organ (kidney) and non-target organs compared with the CS/RM group (Supplementary Fig. 8a–z). The anti-Mb RabMab immune complexes do not cause systemic endothelial toxicity. Taken together, anti-Mb RabMAb migrates to the damaged muscles and kidneys and does not produce apparent toxic adverse effects on the body's vital organs within 14 d of injection.

Anti-Mb RabMAb has stable therapeutic effects within 14 days on AKI and relieves renal fibrosis

In vivo, fluorescence imaging showed that anti-Mb RabMAb was almost wholly metabolized in RM/CS-AKI mice after injection 14 d, and the $T_{1/2}$ of the anti-Mb RabMAb was about 8-11 d in mice. So, we wonder if the nephroprotective effect of anti-Mb RabMAb can be maintained for 14 d. Therefore, we focused on the renal changes at 7 d and 14 d after anti-Mb RabMAb administration (Fig. 6a). Results showed that the contents of BUN, Cr, CK, and Mb in blood and the mRNA levels of *Ngal* and *Kim-1* in the kidney were decreased at 7 d and 14 d after injection of anti-Mb RabMAb compared with RM-AKI mice (Fig. 6b–g). Subsequently, we monitored the constant changes of GFR in mice for 14 d. GFR of RM-AKI mice recovered slightly from 16 h to 24 h after injury, but then showed a continuous downward trend and decreased almost to zero at 7 d. The GFR of the RM-AKI + PBS group slightly improved before 36 h, but the GFR value decreased to the same level as that of the RM-AKI group at 72 h. The GFR of the RM-AKI + Ab group continued to rise after the injection of anti-Mb RabMAb, reaching the highest level after 24 h, which was almost close to that of the NC group and then continued to maintain an excellent renal function within 14 d (Fig. 6h–l). Meanwhile, there was almost no Mb accumulation in the kidneys of the RM-AKI + Ab group at 7 d and 14 d, and the expression of NGAL was also markedly decreased (Fig. 6m). In addition, the RM-AKI and RM-AKI + PBS group had severe fibrosis as assessed by Masson staining and collagen III deposits (Fig. 6n, o and Supplementary Fig. 9a, b). However, the kidneys of the RM-AKI + Ab group were similar to those of the NC group and showed no prominent fibrosis (Fig. 6n, o and Supplementary Fig. 9a, b). Overall, these results indicated that anti-Mb RabMAb could significantly and consistently improve renal function and alleviate renal fibrosis in RM-AKI mice.

Discussion

Early on-site treatment to remove key pathogenic toxic factors K^+ and Mb in the blood as soon as possible is essential to reduce mortality and improve the prognosis of RM/CS-AKI patients[38]. From the perspective of lowering blood K^+, ZS-9 (trade name Lokelma™) has been approved in the European Union and the United States as an oral suspension for treating acute hyperkalemia in adults[39,40]. Lokelma™ may be a potential measure to control the hyperkalemia problem of RM/CS-AKI in emergencies, but the excess free Mb in peripheral blood circulation remains unresolved. Recently, the European Union approved extracorporeal cytokine adsorber CytoSorb® (Cytosorbents Corporation, Monmouth Junction, NJ, USA) may intercept part of the Mb[41,42]. However, CytoSorb® is device-dependent, non-specific[42] (10–55 KD size-selective removal), limited capacity[43] (adsorption capacity decreases to about 10% after 8 h), and uncertain therapeutic efficacy[41].

Since the critical pathogenic factor of RM/CS-AKI is excessive free Mb in blood circulation. Based on the concept of creating a "mobile barrier" to protect the glomerular filtration barrier, we developed an anti-Mb RabMAb[36], which has broad species reactivity (mouse, rat, rabbit, human, and horse) (Supplementary Fig. 1a, b)[36], excellent affinity ($K_D = 0.9409$ pM, Supplementary Fig. 1e), and strong stability (less degradation over 28 d at 25 °C, excellent freeze-thaw resistance (Supplementary Fig. 1f, g). In fact, in recent years, researchers have leveraged the ultra-high affinity of rabbit-derived antibodies to develop more sensitive detection reagents[44,45] and more effective therapeutic drugs for heart transplantation[46] and neonatal pathogen infection[47], etc. In our research, a single dose of anti-Mb RabMAb injection is sufficient for emergency rescue in both

https://doi.org/10.1038/s41467-025-56353-4

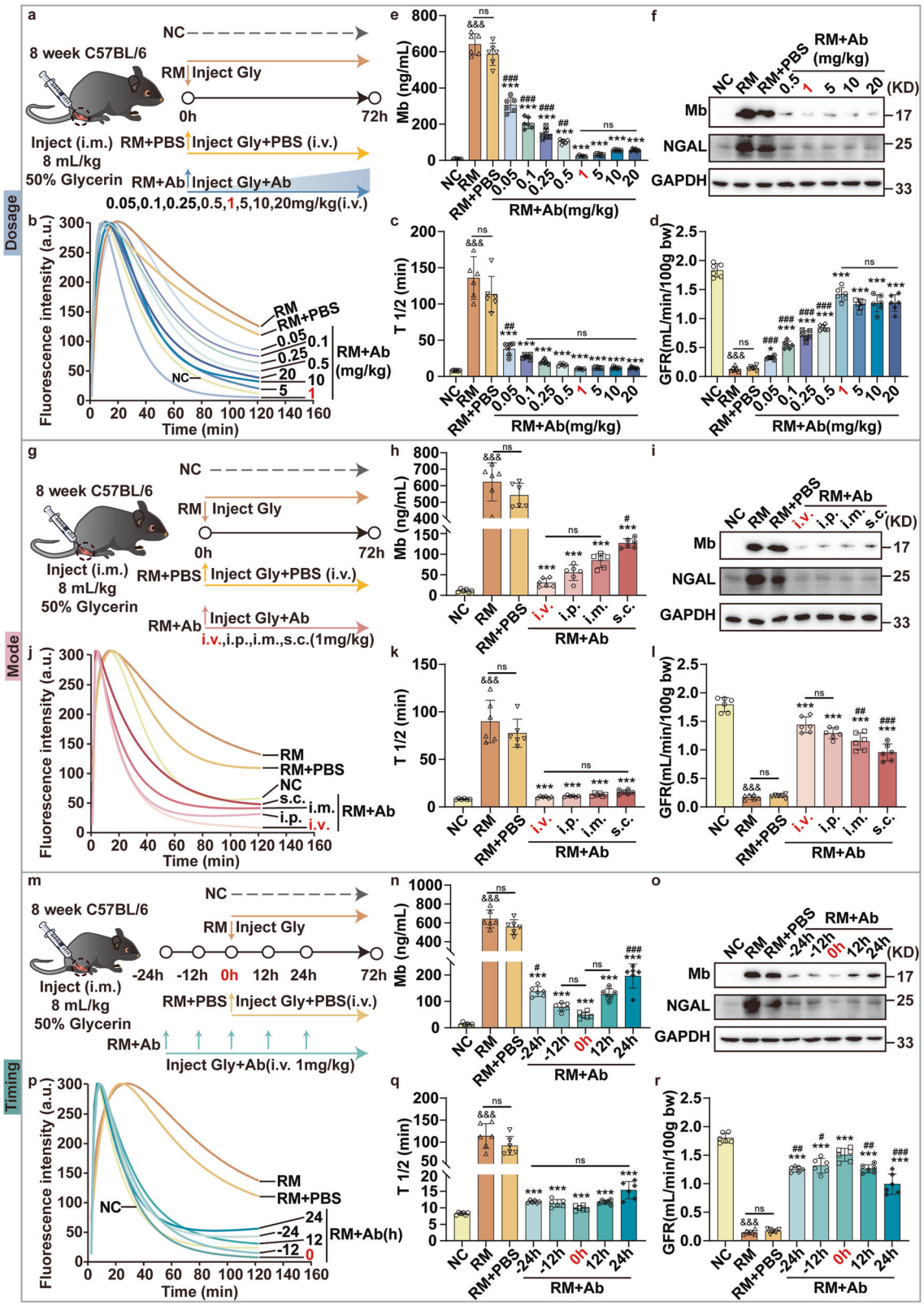

homologous and heterologous RM/CS-AKI animal models (Figs. 1 and 2, Supplementary Fig. 2 and Fig. 3). Antibody therapy is effective because anti-Mb RabMAb specifically binds to the excess free Mb in the blood circulation, thereby reducing the Mb accumulated in the kidneys (Figs. 1d–g, k, o, 2d-k and Supplementary Figs. 2a, b, d, e, 3a, d). The direct or indirect effect of the reduction of toxic Mb reduces glomerular permeability and tubular damage in rhabdomyolysis (Supplementary Fig. 3k). Meanwhile, anti-Mb RabMAb was engulfed by macrophage cells after binding to Mb, and the signal of anti-Mb RabMAb was still significant after Mb was wholly degraded by the cells (Fig. 3g, h and Supplementary Fig. 4). The complex FcRn-mediated IgG recycling pathway may play an essential role in slowly decreasing IgG levels in serum[48]. It is to be regretted that we did not further demonstrate this phenomenon of anti-Mb

Fig. 4 | Exploring the optimal administration dosage, mode, and timing of anti-Mb RabMAb therapy for RM-AKI model mice. a, **g**, **m** Experimental design diagram of anti-Mb RabMAb treatment for RM-AKI model mice on administration dosage, mode, and timing. **e**, **h**, **n** Mb concentration in mice serum. **f**, **i**, **o** WB detection of NGAL expression and Mb accumulation in mice kidneys. GAPDH was used as the loading control. $n = 3$ biological replicates for each group. (**b**, **j**, **p**) Representative images of transcutaneous disappearance curves of FITC-sinistrin excretion. The *x*-axis represents time, the *y*-axis represents the relative transcutaneous fluorescence. **c**, **k**, **q** Terminal half-life ($T_{1/2}$) of FITC-sinistrin excretion. **d**, **l**, **r** GFR values of each group of mice were calculated from the $T_{1/2}$ of FITC-sinistrin. Graph bars represent mean ± SD, and dots indicate individual data points for $n = 6$ for biological replicates per group in (**c**–**e**, **h**, **k**, **l**, **n**, **q**, **r**). One-way ANOVA for (**c**–**e**, **h**, **k**, **l**, **n**, **q**, **r**) followed by Tukey's multiple comparisons test was used to identify the differences.$^{*}p < 0.05$, $^{**}p < 0.01$, $^{***}p < 0.001$ compared with RM group. $^{\#}p < 0.05$, $^{\#\#}p < 0.01$, $^{\#\#\#}p < 0.001$ compared with RM+Ab group (including 1 mg/kg Ab dosage, i.v. mode, 0 h timing). $^{\&}p < 0.05$, $^{\&\&}p < 0.01$, $^{\&\&\&}p < 0.001$ compared with NC group. ns: no significance. The exact *p*-value can be found in the Source Data file. Source data are provided as a Source data file.

RabMAb being re-released to the extracellular space. However, it still proves to some extent that anti-Mb RabMAb will not be rapidly degraded like Mb. Pharmacokinetic analysis revealed that the terminal half-life ($T_{1/2}$) of anti-Mb RabMAb ranged from 8 to 11 days in mice (Fig. 5g), which is within the expected range found for other murine MAbs in mice (6–8 days)[49]. An immune response of animals toward heterologous antibodies can be expected and is reported to be associated with the accelerated clearance of monoclonal antibodies in the serum[50,51]. In the later stage, modification of the Fc region can be considered to extend its serum terminal half-life of anti-Mb RabMAb.

Our results showed that anti-Mb RabMAb administered via the i.v., i.p., i.m., or s.c. all have significant therapeutic effects in RM-AKI mice (Fig. 4g–l and Supplementary Fig. 5g–l). So, the anti-Mb RabMAb is convenient to implement in emergency rescue, especially in disaster situations. Moreover, the timing of antibody injection is more flexible (24 h before decompression to 24 h after decompression), which has the dual effect of prevention and treatment (Fig. 4m–r and Supplementary Fig. 5m–r). The closer to the modeling time point of administration, the better the therapeutic effect will be. Interestingly, a single dose of PBS treatment exhibited a modest protective effect on the kidney within 24 h in the mild RM-AKI model (Fig. 2l, n, o) but not in the severe CS-AKI model (Fig. 2p, r, s). These results underscore the importance of different models and 100 μL PBS administration should not be equated with traditional fluid resuscitation (maybe up to 10 L with 48 h for humans)[52]. Although the dose of 0.05 mg/kg anti-RabMAb group has reached statistical significance compared with the RM group, it might not have biological significance (Fig. 4a–e). This is because GFR values greater than 0.5 are generally considered to have an improvement effect in mice. Therefore, the lower limit of the efficacy of anti-Mb RabMAb i.v. administration in mice is 0.1 mg/kg (Fig. 4a–e). Define the lower limits of efficacy and the upper limits of safety, which are crucial for clinical translation. The no-observed-adverse-effect level (NOAEL) is a generally accepted benchmark for safety when derived from appropriate animal studies and can serve as the starting point for determining a reasonably safe starting dose of a new therapeutic in healthy (or asymptomatic) human volunteers[53] Therefore, the next step needs to do is to determine the value of NOAEL.

Xenogeneic antibodies are prevalent in emergencies in clinical practice, such as equine serum tetanus antitoxin, equine tetanus immunoglobulin, and antivenom (Snake Antivenins). Our findings proved that the anti-Mb RabMAb efficacy in slowing down renal fibrosis and stable improved renal function in heterologous RM/CS-AKI model mice (Fig. 6 and Supplementary Fig. 9). Meanwhile, no damage of major organs in short-time (6 h, 24 h, and 72 h) or 14 d (Fig. 6 and Supplementary Figs. 7, 8). In other words, no acute adverse effects in target and non-target organs, enhancing the clinical translation possibility of the anti-Mb RabMAb. Therefore, anti-Mb RabMAb is suitable for use in emergency treatment.

In summary, a single dose of anti-Mb RabMAb injection immediately after decompression (optimal 1 mg/kg, i.v.) alleviated RM/CS-AKI by blocking Mb from crossing the glomerular filtration barrier and promoted phagocytosis of Mb in both homologous (rabbit) and heterologous (mouse) animal models, which can last for at least 14 d, far exceeding the "72-hour gold time window" of emergency rescue (Fig. 7). In the future, anti-Mb RabMAb can treat RM/CS-AKI and even other diseases related to free Mb in blood circulation.

Methods

Ethics statement

This research complies with all relevant ethical regulations. The animal experiments were approved by the Animal Ethical and Welfare Committee at the Institute of Radiation Medicine, Chinese Academy of Medical Sciences & Peking Union Medical College (NO. IRM-DWLL-2021113, NO. IRM-DWLL-2022195) and Animal Ethical and Welfare of Tianjin University (NO. TJUE-2022-279).

Animal models

New Zealand white rabbits (about 2 kg, 6 months old, male) and C57BL/6 J male mice (about 20 g, 8–10 weeks old) were purchased from Charles River Laboratories (CRL) and SPF (Beijing) Biotechnology Co., Ltd., separately. During the experiment, all animals were housed in a pathogen-free environment with a 12 h light/dark cycle and free access to standard laboratory chow (Jiangsu Xietong Pharmaceutical Bio-engineering Co, Ltd, Nanjing, China, #XTI01WC-009 for mice, #XTC04WC-004 for rabbits) and sterilized water. The ambient temperature was maintained at 21–24 °C and 40–60% humidity for mice and at 20–26 °C and 40–70% humidity for rabbits. After the experiment, the animals were anesthetized until they lost consciousness, and then their blood was collected and euthanized. All rabbits and mice were randomly divided into different groups. For the model of rhabdomyolysis, 8 mL/kg of 50% glycerol was then intramuscularly injected into both hind limbs of rabbits and mice equally, and all rabbits and mice were given free access to water and food. NC group rabbits and mice were intramuscularly injected with physiological saline of the same volume as glycerol. After glycerol injection, the RM-AKI + Ab group rabbits were intravenously injected with 2.5 mg/kg anti-Mb RabMAb. While the RM-AKI + Ab group mice were administered different dosages of anti-Mb RabMAb (0.05, 0.1, 0.25, 0.5, 1, 5, 10, and 20 mg/kg) via different routes (i.v., i.p., i.m., s.c.) within 24 h before and after glycerol injection. The RM-AKI + PBS group mice were injected intramuscularly with glycerol and then intravenously with PBS of the same volume as antibodies.

For preparing the rabbit's CS model, after anesthesia, the digital crush platform was used to continuously crush both hind limbs of rabbits under a pressure of 20 kg for 6 h. CS-AKI + Ab group rabbits were intravenously injected with 2.5 mg/kg anti-Mb RabMAb immediately after decompression. For the mice CS model, after anesthesia, the digital crush platform was used to continuously crush both hind limbs of mice under a pressure of 1.5 kg for 16 h[54]. CS-AKI + Ab group mice were intravenously injected with 1 mg/kg anti-Mb RabMAb immediately after decompression. The CS-AKI + PBS group mice were immediately given intravenous injections of PBS of the same volume as the antibody after decompression. The NC group rabbits and mice were not subjected to any treatment.

Cell culture and cell viability

Mouse tubular epithelial cells (TECs) TCMK-1 (Servicebio, #STCC20015G) and mouse mononuclear macrophage cells RAW 264.7

https://doi.org/10.1038/s41467-025-56353-4

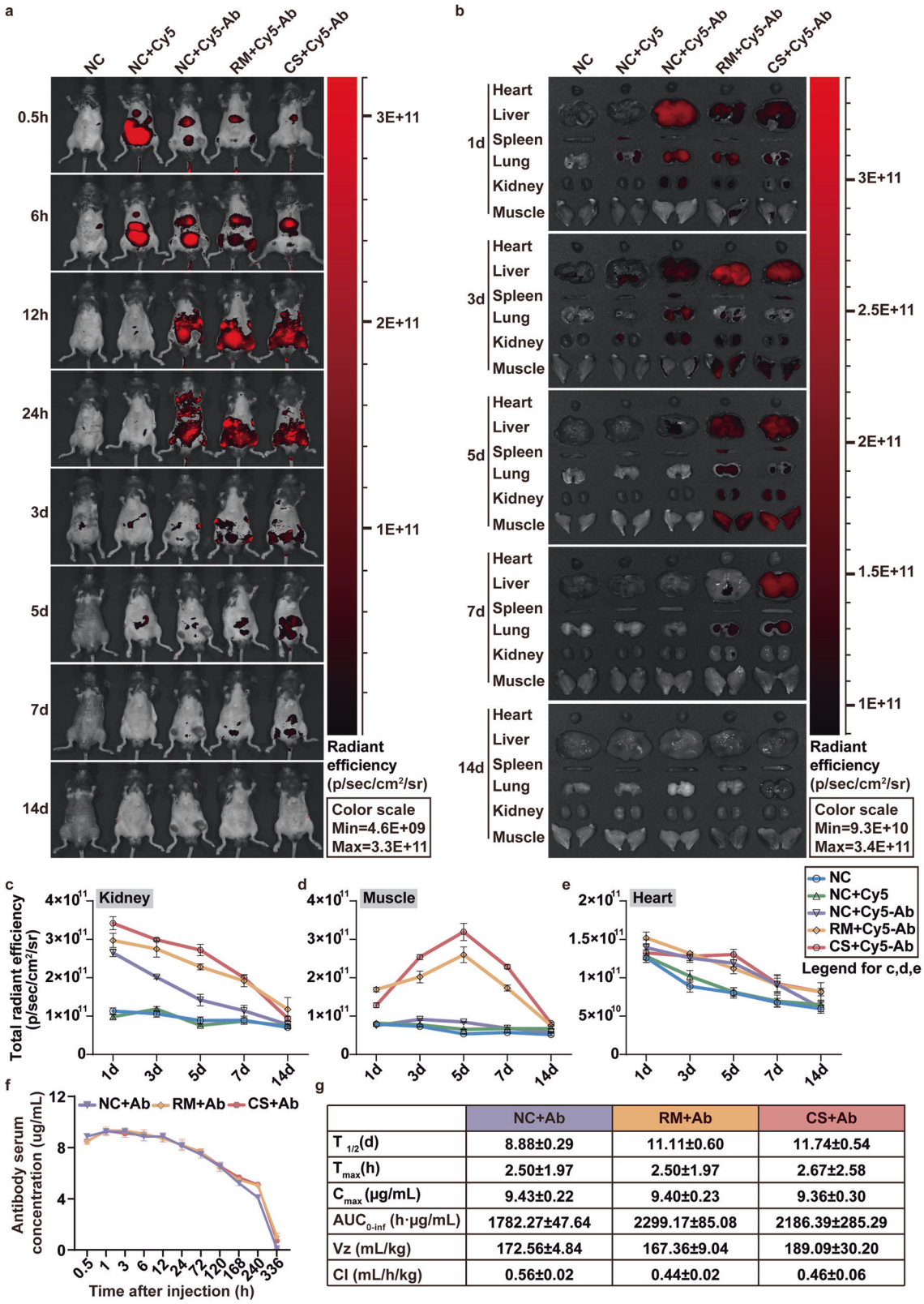

	NC+Ab	RM+Ab	CS+Ab
$T_{1/2}$(d)	8.88±0.29	11.11±0.60	11.74±0.54
T_{max}(h)	2.50±1.97	2.50±1.97	2.67±2.58
C_{max} (μg/mL)	9.43±0.22	9.40±0.23	9.36±0.30
$AUC_{0\text{-}inf}$ (h·μg/mL)	1782.27±47.64	2299.17±85.08	2186.39±285.29
Vz (mL/kg)	172.56±4.84	167.36±9.04	189.09±30.20
Cl (mL/h/kg)	0.56±0.02	0.44±0.02	0.46±0.06

(Servicebio, #STCC20020G) were cultured in DMEM-high glucose medium (Sparkjade, #CA0002) containing 10% FBS and antibiotics (100 U/mL penicillin and 0.1 mg/mL streptomycin) (Solarbio, #P1400) at 37 °C in humidified air with 5% CO_2. TCMK-1 cells were inoculated in 96-well plates (NEST, #701002) at a concentration of 5×10^3 cells/well for 24 h. Cells were treated with graded concentrations of mouse ferrous Mb (25, 50, 100, 200, 400, 800 μM) for 6 h. Then, cells were co-incubated with CCK8 solution (YEASEN, #40203ES60) in a culture incubator for 2 h, and the optical density (OD) values were detected at 450 nm by Microplate Reader (BioTek, Epoch 2). Based on the detection results of CCK8, we ultimately used 200 μM mouse ferrous Mb treated TCMK-1 cells at the exponential growth phase to mimic the RM/CS-AKI model in vitro. Furthermore, to investigate the phagocytic effect of macrophages on Mb and anti-Mb RabMAb, 200 μM mouse

Fig. 5 | The organ distribution of anti-Mb RabMAb in RM/CS-AKI mice. a In vivo fluorescence imaging of RM/CS-AKI mice treated with single intravenous administration of Cy5 and Cy5 labeled anti-Mb RabMAb (1 mg/kg) at different time points (0.5 h, 6 h, 12 h, 24 h, 3 d, 5 d, 7 d and 14 d). $n = 3$ for biological replicates per group. **b** Fluorescence images of major organs of RM/CS-AKI mice treated with single intravenous administration of Cy5 and Cy5 labeled anti-Mb RabMAb (1 mg/kg) at different time points (1 d, 3 d, 5 d, 7 d, and 14 d). $n = 3$ for biological replicates per group. **c**–**e** The fluorescence intensity in the kidney, muscle, and heart after the mice injected with Cy5 and Cy5 labeled anti-Mb RabMAb (1 mg/kg) at different time points (1 d, 3 d, 5 d, 7 d, and 14 d). $n = 3$ for biological replicates per group. Results are presented as means ± SD. **f** The plasma concentration-time profiles of anti-Mb RabMAb after a single dose i.v. administration in mice. **g** Mean pharmacokinetic parameters (± standard deviation (S.D.)) of anti-Mb RabMAb after single dose i.v. administration in mice. $T_{1/2}$, terminal half-life; T_{max}, the time to reach maximum plasma concentration; C_{max}, the maximum plasma concentration; $AUC_{(inf)}$, the area under the serum concentration-time curve from time 0 to infinity; Vz, the volume of distribution; Cl, plasma clearance. Experiments were conducted independently with six mice in each group in (**f**, **g**). The data points of 0.5 h, 1 h, 3 h, 6 h, and 12 h for $n = 3$ biological replicates with 2 technical replicates in each group. The data points of 24 h, 72 h, 120 h, 168 h, 240 h, and 336 h for $n = 6$ biological replicates in each group. Results are presented as means ± SD. Source data are provided as a Source data file.

ferrous Mb was used to treat RAW 264.7 cells for 0.5, 1, 2, 4, 6, 8, 12, 24, 36 and 48 h, and then immunofluorescence co-localization was used to analyze the phagocytic effect.

Biochemistry analysis

Serum and urine samples from rabbits and mice were collected. The levels of BUN, Cr, CK, and Mb were detected by an automatic biochemical analysis instrument (iMagic-V 7, Icubio) and commercial assay kits (Derui Biotechnology Co., Ltd.).

Hematoxylin-Eosin (HE)

Mouse or rabbit organs were fixed in 4% paraformaldehyde (Servicebio, #G1101), embedded in paraffin, and sectioned into 4 μm thickness. After staining with Hematoxylin-Eosin (HE) stain kit (Solarbio, #G1120) and dehydration, the optical microscope was used to observe and evaluate the pathological changes in kidney, muscle, heart, liver, and lung tissue.

Immunohistochemistry (IHC)

After dewaxing and hydration, the kidney tissue sections were heated for antigen repair and then incubated with 0.5% Triton X-100 (ACMEC, #T88490) and 3% H_2O_2 for membrane permeability and peroxidase removal. Nonspecific binding sites were blocked with 5% goat serum (Solarbio, #SL038) and incubated with primary antibodies against NGAL (1:300, Affinity, #DF6816), Mb (1:300, Abcam, #ab77232), KIM-1(1:300, ABclonal, #A2831) at 4°C overnight. Then, the sections were incubated with HRP-coupled secondary antibodies at room temperature for 1 h. The sections were stained with a DAB kit (Solarbio, #DA1015), and cell nuclei were stained with hematoxylin. Finally, kidney tissue sections were observed under an optical microscope.

Immunofluorescence (IF)

The pre-treatment method for tissue immunofluorescence is the same as immunohistochemistry. For cellular immunofluorescence, TCMK-1 and RAW 264.7 cells were inoculated on a glass cover slide in a 24-well plate (NEST, #702002), fixed with 4% paraformaldehyde (Servicebio, #G1101), then permeated with 0.5% Triton X-100 and sealed with 5% BSA (Solarbio, #A8010) at room temperature. Then the tissue slices or cell slides were incubated with primary antibodies against Mb (1:500, Santa Cruz, #sc-74525) and fluorescein-labeled LTL (1:300, Vector laboratories, #FL-1321-2) at 4 °C overnight and secondary antibodies coupled to Alexa Fluor 488/594 (1:200, ZSGB-BIO, #ZF-0511 and #ZF-0513) at room temperature for 1 h. The cell nuclei were stained by 4′,6-diamidino-2-phenylindole (DAPI) (Solarbio, #C0060) in the dark. Finally, the slides were observed using confocal microscopy (Nikon, A1).

Quantitative real-time PCR (qPCR)

The total RNA of kidney tissues was extracted by TRIeasy™ LS Total RNA Extraction Reagent (YEASEN, #19201ES60), while Nanodrop One was used to detect RNA purity and concentration. Reverse transcription into cDNA was performed using the Hifair®III 1st Strand cDNA Synthesis Kit (YEASEN, #11139ES10). Then the Hieff® qPCR SYBR Green Master Mix (No Rox) kit (YEASEN, #11201ES03) was used to perform qPCR with the LightCycler® 96 instrument (Roche). The relative expression level was calculated by $2^{-\Delta\Delta Ct}$. Primers are listed in Supplementary Table 1.

Western blotting (WB)

Cold RIPA lysis buffer containing protease inhibitor was used to extract protein from kidney tissue. The samples were quantified with the BCA protein quantification kit (YEASEN, #20201ES76). The 30 μg total protein was separated by SDS-PAGE and transferred to PVDF membranes. After blocking with 5% skimmed milk (Sparkjade, #ED0019) at room temperature, then the membranes were incubated with primary antibodies against NGAL (1:2000, Santa Cruz, #sc-74525), Mb (1:5000, Abcam, #ab77232), and GAPDH (1:10000, BOSTER, #BM1623) overnight at 4 °C. Then, the membranes were incubated with HRP-coupled secondary antibodies at room temperature. The protein bands were visualized with enhanced ECL chemiluminescent substrate kit (YEASEN, #36222ES60) and imaged with Tanon 5200 Multiple Detection System.

Immunoprecipitation (IP)

Extracted the total protein from the renal tissue of RM/CS-AKI mice using IP lysis buffer, incubated it with protein A magnetic beads (Bimake, #B23202), and added rabbit anti-Mb monoclonal antibody/rabbit anti-IgG antibody (Abcam, #ab172730) to incubate overnight at 4 °C. Subsequent WB analysis was performed using IP samples.

Surface plasmon resonance (SPR)

The affinity between His-Mb protein and anti-Mb RabMAb was measured at room temperature using a Biacore T200 SPR instrument. The anti-Mb RabMAb first binds to the protein A chip (GE Healthcare). Then, gradient concentrations of His-Mb protein flowed over the chip surface. After each cycle, the sensor surface was regenerated. The data was collected, and the affinity was calculated. The running buffer used for ligand attachment and analyte-binding experiments was 0.01 M PBS buffer with 2 mM KH_2PO_4, 8 mM $Na_2HPO_4{\cdot}12H_2O$, 136 mM NaCl, 2.6 mM KCl, adjusted to pH 7.4.

Glomerular filtration rate (GFR) assessment and calculation

Transcutaneous GFR was measured and performed as previously reported[55,56]. A miniaturized imager device (MediBeacon™ Inc.) was mounted onto the shaved back of mice. The background signal of the skin was recorded for 5 min. Then, a single dose of FITC-stingrin (i.v., 70 mg/kg BW) (MediBeacon™ Inc.) was injected into mice. After collecting signals for 1.5–2 h, the imaging device MPD Studio software (MediBeacon™ Inc.) analyzed data. GFR was calculated as follows: GFR [μl/min/100 g body weight] = 14616.8 [μl/100 g body weight]/$t_{1/2}$ (FITC-sinistrin) [min].

Fluorescence imaging of Cy5 labeled anti-Mb RabMAb in vivo

Label the anti-Mb RabMAb with Cy5 dye and inject them into the anesthetized and shaved mice of NC + Cy5-Ab, RM + Cy5-Ab, and CS + Cy5-Ab groups via tail vein at a dose of 1 mg/kg. Use small animal live imaging equipment (Tanon, ABL-X5) to perform in vivo fluorescence

https://doi.org/10.1038/s41467-025-56353-4

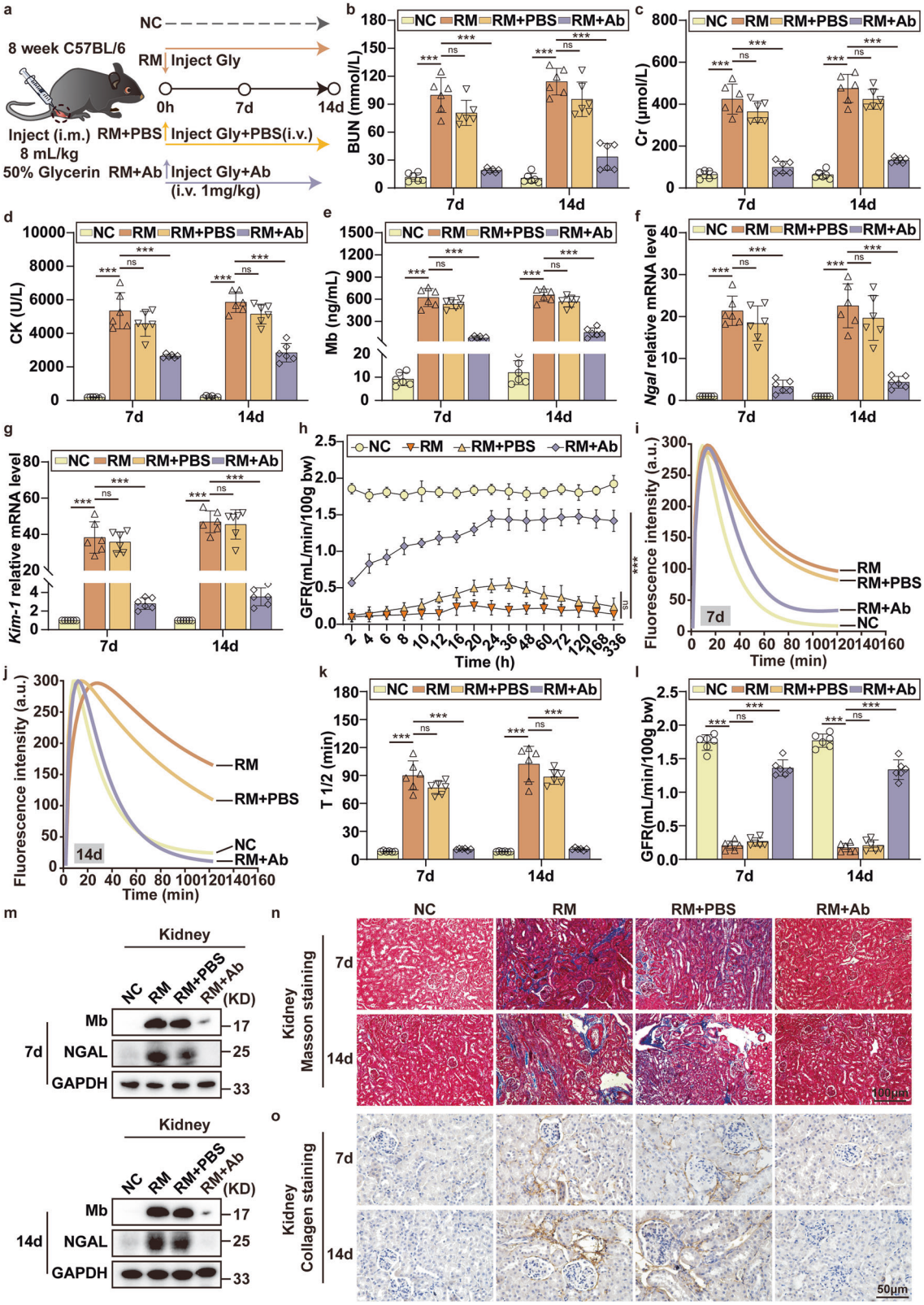

scanning imaging at different time points after injection (0.5 h, 6 h, 12 h, 24 h, 3 d, 5 d, 7 d, 14 d). Perform fluorescence intensity analysis on whole-body images. After 1 d, 3 d, 5 d, 7 d, and 14 d of injection of labeled antibodies, the mice were euthanized. The major organs and tissues (heart, liver, spleen, lung, kidney, and muscle) were dissected and collected for fluorescence imaging, and the corresponding fluorescence intensity was calculated.

Pharmacokinetic statistical analysis in mice

The male C57/BL mice were divided into NC, RM-AKI, and CS-AKI groups (6 mice per group). Intravenous injection of 1 mg/kg anti-RabMAb. Blood samples of approximately 100 μL were collected before injection, and at 0.5 h, 1 h, 3 h, 6 h, 12 h, 24 h, 3 d, 5 d, 7 d, 10 d, and 14 d (in some of the mice) after administration. Anti-RabMAb blood levels were assessed with a specific ELISA assay as previously

Fig. 6 | Anti-Mb RabMAb therapy slows down renal fibrosis and stable improves renal function within 14 days. a Experimental design diagram of anti-Mb RabMAb treatment for RM-AKI model mice. **b**–**e** BUN, Cr, CK, and Mb concentration in mice serum. **f**, **g** qPCR analyses the mRNA level of kidney injury markers *Kim-1* and *Ngal* in the kidney. **h** GFR values of each group of mice were calculated from the terminal half-life ($t_{1/2}$) of FITC-sinistrin. Data are presented as mean ± SD. $n = 3$ biological replicates for each group. One-way ANOVA followed by Tukey's multiple comparisons test was used to identify the differences. (**i**, **j**) Representative images of transcutaneous disappearance curves of FITC-sinistrin excretion. The *x*-axis represents time, the *y*-axis represents the relative transcutaneous fluorescence. **k** $T_{1/2}$ of FITC-sinistrin excretion. **l** GFR values were calculated from the $T_{1/2}$ of FITC-sinistrin. **m** WB detection of NGAL expression and Mb accumulation in the mice kidneys. GAPDH was used as the loading control. $n = 3$ biological replicates for each group. **n** Masson staining of kidney sections showed the distribution of collagen (blue) at 7 d and 14 d in different groups. $n = 3$ for biological replicates. **o** Collagen III Immunohistochemistry staining of kidney sections showed the Collagen III deposition at 7 d and 14 d in different groups. $n = 3$ for biological replicates. Graph bars represent mean ± SD, and dots indicate individual data points for $n = 6$ for biological replicates per group in (**b**–**g**, **k**, **l**). Two-way ANOVA for (**b**–**g**, **k**, **l**) followed by Tukey's multiple comparisons test was used to identify the differences. * $p < 0.05$, ** $p < 0.01$, *** $p < 0.001$, ns: no significance. The exact *p*-value can be found in the Source Data file. Source data are provided as a Source data file.

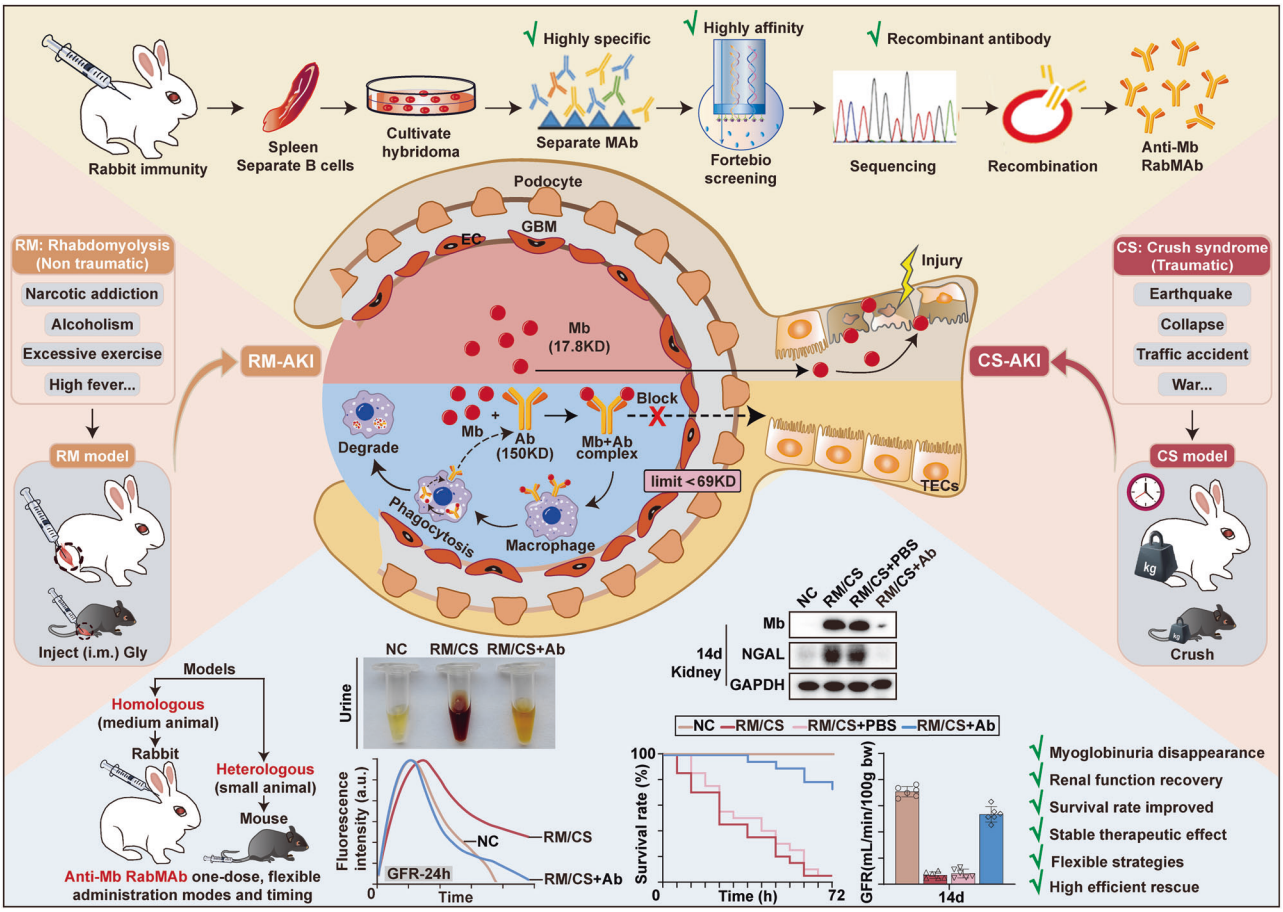

Fig. 7 | Schematic diagram of anti-Mb RabMAb treatment for RM/CS-AKI. A novel strong specificity, excellent affinity, superior stability, and broad species reactivity recombination anti-Mb rabbit monoclonal antibody (RabMAb) was developed. Anti-Mb RabMAb (~150 KD) one-dose injection alleviated RM/CS-AKI by blocking the free Mb (~17 KD) in the blood circulation from passing through the glomerular filtration barrier (~69 KD) and promotes phagocytosis of Mb in both homologous (rabbit) and heterologous (mouse) animal models. Anti-Mb RabMAb has a stable therapeutic effect for at least 14 d or more.

described with minor modifications and derived concentrations were used to generate pharmacokinetic profiles versus time. From the plasma concentration-time profiles, the maximum plasma concentration (C_{max}) and the time to reach C_{max} (T_{max}) were obtained. All pharmacokinetic analyses were done using Phoenix WinNonlin 8.3.5 (Certara Software) to estimate terminal half-life ($T_{1/2}$), area under the serum concentration-time curve from time 0 to infinity [$AUC_{(inf)}$], volume of distribution (Vz), and plasma clearance (CI).

Statistical analysis

Continuous variables with normal distribution were presented as mean ± standard deviation (SD). For more than two groups, one-way ANOVA or two-way ANOVA followed by Tukey's multiple comparisons test were used to identify the differences. Underlying assumptions for these tests, including sample independence, variance equality, and normality were assumed to be met. The cumulative incidence estimate was used to calculate the probability of survival rate as a function of time. The log-rank test was used to compare survival curves. A value of $p < 0.05$ was considered statistical significance. Three levels of statistical significance was set ($^{*/\#/\&}p < 0.05$; $^{**/\#\#/\&\&}p < 0.01$; $^{***/\#\#\#/\&\&\&}p < 0.001$; ns: no significance). GraphPad Prism software was used for data analysis and graph plotting.

Reporting summary

Further information on research design is available in the Nature Portfolio Reporting Summary linked to this article.

Data availability

All data relating to this study can be found in the main text, figures, or Supplementary information. The Source Data Underlying Figs. 1–6 and Supplementary Figs. 1–6, 8, 9 are provided as a Source Data file. Specific data *p*-values are also included within the Source Data file. Additional details on protocols that support the findings of this study will be made available by the corresponding author upon request. Source data are provided in this paper.

References

1. Gao, J., Deng, Q., Yu, J., Wang, C. & Wei, W. Role of renal tubular epithelial cells and macrophages in cisplatin-induced acute renal injury. *Life Sci.* **339**, 122450 (2024).
2. Zheng, Z. L. et al. Mechanism of dexmedetomidine protection against cisplatin induced acute kidney injury in rats. *Ren. Fail.* **46**, 2337287 (2024).
3. Schetz, M. & Prowle, J. Focus on acute kidney injury 2017. *Intensive Care Med.* **44**, 1992–1994 (2018).
4. Bellomo, R., Kellum, J. A. & Ronco, C. Acute kidney injury. *Lancet* **380**, 756–766 (2012).
5. Hebert, J. F., Burfeind, K. G., Malinoski, D. & Hutchens, M. P. Molecular mechanisms of rhabdomyolysis-induced kidney injury: From bench to bedside. *Kidney Int. Rep.* **8**, 17–29 (2023).
6. Zimmerman, J. L. & Shen, M. C. Rhabdomyolysis. *Chest* **144**, 1058–1065 (2013).
7. Weston, M. D., Hirsch, N. P. & Jones, J. A. Narcotic overdose and acute rhabdomyolysis. *Anaesthesia* **41**, 1269 (1986).
8. Haller, R. G. & Drachman, D. B. Alcoholic rhabdomyolysis: an experimental model in the rat. *Science.* **208**, 412–415 (1980).
9. Kelly, R., Semple, D. & Harper, A. Recurrent acute kidney injury with severe loin pain and patchy renal Ischaemia after Anaerobic exercise without renal Hypouricaemia in a New Zealand European male. *Case Rep. Nephrol. Dial.* **11**, 176–182 (2021).
10. Luan, Y. et al. Serum myoglobin modulates kidney injury via inducing ferroptosis after exertional heatstroke. *J. Transl. Intern. Med.***11**, 178–188 (2023).
11. De Santo, N. G., Bisaccia, C., DeSanto, L. S., Cucu, A. I. & Costea, C. F. John XXI, the pope philosopher and physician-scientist of portuguese origins died of crush syndrome in 1277. *J. Relig. Health* **60**, 1305–1317 (2021).
12. Bywaters, E. G. & Beall, D. Crush injuries with impairment of renal function. 1941. *J. Am. Soc. Nephrol.* **9**, 322–332 (1998).
13. Kasatkin, V. N., Kanaeva, E. S., Maetnikov, A., Rumiantsev, A. G. & Blokhin, B. M. [Endotoxemia in crush syndrome]. *Khirurgiia* **4**, 43–44 (1995).
14. Li, W. et al. Management of severe crush injury in a front-line tent ICU after 2008 Wenchuan earthquake in China: an experience with 32 cases. *Crit.Care* **13**, R178 (2009).
15. Reingardienė, D., Jodžiūnienė, L. & Lažauskas, R. [Muscle crush injury and crush syndrome]. *Medicina* **46**, 435–441 (2010).
16. Yalçınkaya Yavuz, Ö., Aydoğdu, N., Taştekin, E. & Süt, N. The effects of baicalin on myoglobinuric acute renal failure in rats. *Balkan Med. J.* **35**, 68–76 (2018).
17. Luo, G. et al. An over-the-horizon potential safety threat vehicle identification method based on ETC big data. *Heliyon* **9**, e20050 (2023).
18. Bartels, S. A. & Vanrooyen, M. J. Medical complications associated with earthquakes. *Lancet* **379**, 748–757 (2012).
19. Bilham, R. Earthquakes and urban growth [4]. *Nature* **336**, 625–626 (1988).
20. Disel, N. R. et al. Factors affecting the mortality of February earthquakes victims in Türkiye. *Am J. Emerg. Med.* **77**, 115–120 (2023).
21. Abu-Zidan, F. M., Jawas, A., Idris, K. & Cevik, A. A. Surgical and critical care management of earthquake musculoskeletal injuries and crush syndrome: A collective review. *Turk. J. Emerg. Med.* **24**, 67–79 (2024).
22. Hertzberg, D., Rydén, L., Pickering, J. W., Sartipy, U. & Holzmann, M. J. Acute kidney injury-an overview of diagnostic methods and clinical management. *Clin. Kidney J.* **10**, 323–331 (2017).
23. Yu, J. G. et al. Anisodamine ameliorates hyperkalemia during crush syndrome through estradiol-induced enhancement of insulin sensitivity. *Front. Pharmacol.* **10**, 1444 (2019).
24. Petejova, N. & Martinek, A. Acute kidney injury due to rhabdomyolysis and renal replacement therapy: a critical review. *Crit. Care* **18**, 224 (2014).
25. Wang, P. T. et al. RIG-I, a novel DAMPs sensor for myoglobin activates NF-κB/caspase-3 signaling in CS-AKI model. *Mil. Med. Res.* **8**, 37 (2021).
26. Qiao, O., Wang, X., Wang, Y., Li, N. & Gong, Y. Ferroptosis in acute kidney injury following crush syndrome: A novel target for treatment. *J. Adv. Res.* **54**, 211–222 (2023).
27. Moore, K. P. et al. A causative role for redox cycling of myoglobin and its inhibition by alkalinization in the pathogenesis and treatment of rhabdomyolysis-induced renal failure. *J. Biol. Chem.* **273**, 31731–31737 (1998).
28. Zager, R. A., Johnson, A. C. & Becker, K. Plasma and urinary heme oxygenase-1 in AKI. *J. Am. Soc. Nephrol.* **23**, 1048–1057 (2012).
29. Sever, M. S., Vanholder, R. & Lameire, N. Management of crush-related injuries after disasters. *N. Engl. J. Med.* **354**, 1052–1063 (2006).
30. Bruso, J. R. et al. Rhabdomyolysis and hyponatremia: A cluster of five cases at the 161-km 2009 western states endurance run. *Wilderness Environ. Med.* **21**, 303–308 (2010).
31. Li, X. et al. Earlier continuous renal replacement therapy is associated with reduced mortality in rhabdomyolysis patients. *Ren. Fail.* **44**, 1743–1753 (2022).
32. Collins, A. J. Kidney dialysis treatment for Victims of the Armenian Earthquake. *N. Engl. J. Med.* **320**, 1291–1292 (1989).
33. Zhang, B. F. et al. Anti-high mobility group box-1 (HMGB1) antibody attenuates kidney damage following experimental crush injury and the possible role of the tumor necrosis factor-α and c-Jun N-terminal kinase pathway. *J. Orthop. Surg. Res.* **12**, 110 (2017).
34. Matsumoto, H. et al. Therapeutic effectiveness of Anti-RAGE antibody administration in a rat model of crush injury. *Sci. Rep.* **7**, 12255 (2017).
35. Shimazaki, J. et al. Systemic involvement of high-mobility group box 1 protein and therapeutic effect of anti-high-mobility group box 1 protein antibody in a rat model of crush injury. *Shock* **37**, 634–638 (2012).
36. Wang, X., Qiao, O., Han, L., Li, N. & Gong, Y. A novel rabbit anti-myoglobin monoclonal antibody's potential application in rhabdomyolysis associated acute kidney injury. *Int. J. Mol. Sci.* **24**, 7822 (2023).
37. Wang, S. et al. Erythropoietin protects against rhabdomyolysis-induced acute kidney injury by modulating macrophage polarization. *Cell Death Dis.* **8**, e2725 (2017).
38. Sarı, H., Özel, M., Akkoç, M. F. & Şen, A. First-week analysis after the Turkey Earthquakes: demographic and clinical outcomes of victims. *Prehos. Disaster Med.* **38**, 294–300 (2023).
39. Meaney, C. J., Beccari, M. V., Yang, Y. & Zhao, J. Systematic review and meta-analysis of patiromer and Sodium Zirconium Cyclosilicate: A new armamentarium for the treatment of hyperkalemia. *Pharmacotherapy* **37**, 401–411 (2017).
40. Hoy, S. M. Sodium Zirconium Cyclosilicate: A review in hyperkalaemia. *Drugs* **78**, 1605–1613 (2018).
41. Dilken, O. et al. Successful reduction of creatine kinase and myoglobin levels in severe rhabdomyolysis using extracorporeal blood purification (CytoSorb®). *Blood Purif.* **49**, 743–747 (2020).

42. Jerman, A., Andonova, M., Persic, V. & Gubensek, J. Extracorporeal removal of myoglobin in patients with rhabdomyolysis and acute kidney injury: Comparison of high and medium cut-off membrane and an adsorber cartridge. *Blood Purif.* **51**, 907–911 (2022).
43. Albrecht, F. et al. Rapid and effective elimination of myoglobin with CytoSorb® hemoadsorber in patients with severe rhabdomyolysis. *Blood Purif.* **53**, 88–95 (2024).
44. Miller, D. L., Potempska, A., Wegiel, J. & Mehta, P. D. High-affinity rabbit monoclonal antibodies specific for amyloid peptides amyloid-β40 and amyloid-β42. *J. Alzheimers Dis.* **23**, 293–305 (2011).
45. Ozawa, T. et al. A novel rabbit immunospot array assay on a chip allows for the rapid generation of rabbit monoclonal antibodies with high affinity. *PloS ONE* **7**, e52383 (2012).
46. Bonaros, N. et al. Ten-year follow-up of a prospective, randomized trial of BT563/bb10 versus anti-thymocyte globulin as induction therapy after heart transplantation. *J. Heart Lung Transplant.* **25**, 1154–1163 (2006).
47. Senn, B. M. et al. Monoclonal antibodies targeting different cell wall antigens of group B streptococcus mediate protection in both Fc-dependent and independent manner. *Vaccine* **29**, 4116–4124 (2011).
48. Igawa, T., Haraya, K. & Hattori, K. Sweeping antibody as a novel therapeutic antibody modality capable of eliminating soluble antigens from circulation. *Immunol. Rev.* **270**, 132–151 (2016).
49. Vieira, P. & Rajewsky, K. The half-lives of serum immunoglobulins in adult mice. *Eur. J. Immunol.* **18**, 313–316 (1988).
50. Schellekens, H. The immunogenicity of therapeutic proteins. *Discov. Med.* **9**, 560–564 (2010).
51. Schweizer, D. et al. Pharmacokinetics, biocompatibility and bioavailability of a controlled release monoclonal antibody formulation. *J. Control. Release* **172**, 975–982 (2013).
52. Better, O. S. & Stein, J. H. Early management of shock and prophylaxis of acute renal failure in traumatic rhabdomyolysis. *N. Engl. J. Med.* **322**, 825–829 (1990).
53. Department of Health and Human Services Food and Drug Administration. Guidance for industry on estimating the maximum safe starting dose in initial clinical trials for therapeutics in adult healthy volunteers[EB/OL]. https://www.federalregister.gov/d/05-14456 (2005).
54. Li, N. et al. Myoglobin promotes macrophage polarization to M1 type and pyroptosis via the RIG-I/Caspase1/GSDMD signaling pathway in CS-AKI. *Cell Death Discov.* **8**, 90 (2022).
55. Steiger, S. et al. Anti-transforming growth factor β IgG elicits a dual effect on Calcium Oxalate crystallization and progressive nephrocalcinosis-related chronic kidney disease. *Front. Immunol.* **9**, 619 (2018).
56. Cippà, P. E. et al. A late B lymphocyte action in dysfunctional tissue repair following kidney injury and transplantation. *Nat. Commun.* **10**, 1157 (2019).

Acknowledgements

This research was supported by the National Natural Science Foundation of China (No. 82273998, Y.H.G.; No. 32170822, Z.C.L.), and the Ministry of Science and Technology of the People's Republic of China (National Key R&D Program of China, No. 2021YFC3002203, Y.H.G.), CAMS Innovation Fund for Medical Sciences (CIFMS, No. 2023-I2M-2-007, S.Q.R.), Beijing-Tianjin-Hebei Basic Research Cooperation Special Project (No. J230018, S.Q.R.), the Funding of Thinkingbiomed Biotechnology (Beijing) Co., Ltd (No.100406, Z.C.L.). We sincerely thank Prof. Xudong Wu from Tianjin Medical University and Dr. Kunpeng Peng of Unitalen Attorneys at Law for their discussion and advice.

Author contributions

Y.H.G., Z.C.L., N.L., S.Q.R., and X.Y.W. conceived and designed the study. X.Y.W., L.H., and O.Q. performed the experiments. X.Y.W. and N.L. analyzed and interpreted data and drafted the manuscript. N.L. and Y.H.G. revised the manuscript. X.C., P.T.W., and L.C.Z. provided critical reagents and materials. Y.J.H., F.J.B., and H.R.H. analyzed the research data of cells. S.S., L.Z., Z.Z.L., and X.H.D. analyzed the research data of mice. All authors approved the submitted version of the manuscript.

Competing interests

The authors declare no competing interests.

Additional information

Supplementary information The online version contains supplementary material available at https://doi.org/10.1038/s41467-025-56353-4.

Correspondence and requests for materials should be addressed to Ning Li, Shuquan Rao, Zichuan Liu or Yanhua Gong.

Peer review information *Nature Communications* thanks Jung Pyo Lee, Idris Boudhabhay, and the other anonymous reviewer(s) for their contribution to the peer review of this work. A peer review file is available.